Inorganic Chemistry

Article

pubs.acs.org/IC

Structural Consequences of the N7 and C8 Translocation on the Metal Binding Behavior of Adenine

Alicia Domínguez-Martín,*[,†] Duane Choquesillo-Lazarte,[‡] Jose A. Dobado,[∥] Henar Martínez-García,[¶] Luis Lezama,[§] Josefa M. González-Pérez,[†] Alfonso Castiñeiras,[⊥] and Juan Niclós-Gutiérrez[†]

[†]Department of Inorganic Chemistry, Faculty of Pharmacy, University of Granada, E-18071 Granada, Spain

[‡]Laboratorio de Estudios Cristalográficos, IACT, CSIC-Universidad de Granada, Av. de las Palmeras 4, E-18100 Armilla, Granada, Spain

[∥]Grupo de Modelización y Diseño Molecular, Departamento de Química Orgánica, Facultad de Ciencias, Universidad de Granada, E-18071 Granada, Spain

[¶]Departamento de Química Orgánica, Escuela de Ingenierías Industriales, Universidad de Valladolid, E-47071 Valladolid, Spain

[§]Department of Inorganic Chemistry, Faculty of Science and Technology, University of Basque Country, E-48080 Bilbao, Spain

[⊥]Department of Inorganic Chemistry, Faculty of Pharmacy, University of Santiago de Compostela, E-15782 Santiago de Compostela, Spain

Supporting Information

ABSTRACT: 7-Deaza-8-aza-adenine, namely 4-aminopyrazolo[3,4-d]-pyrimidine (H4app), is a bioisoster of adenine (Hade) resulting from the translocation of N7 and C8 atoms on the purine moiety. With the aim of studying the influence of this translocation on the metal binding abilities of H4app, we have prepared and structurally characterized two ternary copper(II) complexes having H4app and one N-benzyl-iminodiacetate chelator (MEBIDA or FBIDA, with a methyl or fluoro group in para- of the benzyl aromatic ring): $[Cu_2(MEBIDA)_2(\mu_2\text{-}N1,N8\text{-}H4app)(H_2O)_2]\cdot 4H_2O$ (**1**) and $[Cu_4(FBIDA)_4(\mu_2\text{-}N8,N9\text{-}H4app)_2(H_2O)]\cdot 3.5H_2O$ (**2**). Furthermore, thermal, spectral, and magnetic properties have been also investigated. In **1**, H(N9)4app is disordered over two equally pondered positions and the μ_2-N1,N8 coordination mode is assisted by N6-H···O and N9-H···O intramolecular interactions, respectively. The acyclic nonlinear molecular topology of **2** is strongly influenced by two intramolecular H-bonding interactions (O-H···O-carboxylate) involving the apical aqua ligand of a terminal Cu(II) atom. Thus, both compounds have in common the Cu−N8 bond. In order to better understand our limited structural information, DFT calculations for the individual tautomers of H4app as well as mononuclear Cu(II) model systems have been carried out. According to previous results, we conclude that H(N9)4app is the most stable tautomer followed by H(N8)4app. When N9 and N8 are metalated, then the tautomer H(N1)4app can come into play as observed in compound **2**. Likewise, the findings concerning compound **1** suggest that the formation of a Cu−N1 bond in H4app results was favored compared to neutral adenine, for which only one case has been reported with such coordination despite the large variety of related Cu(II)-Hade described in the literature.

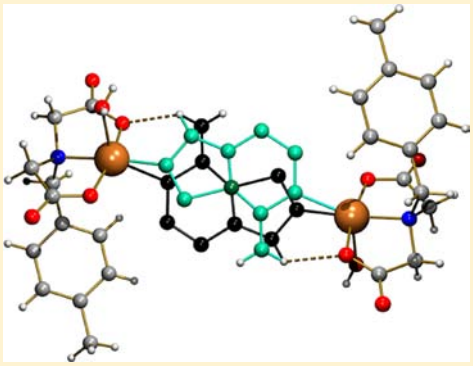

INTRODUCTION

In the last decades, a large number of papers has addressed the metal binding patterns of natural nucleobases as well as closely related ligands.[1] In this sense, our research group has been devoted to the study of adenine, which has proved to be a fairly rich versatile ligand.[2] Moreover, in order to extend the reach of our results, we have also studied several oxo-, amino-, aza-, and/or deaza-purine derivatives.[3] The better understanding of the metal binding patterns of these purine analogues is challenging because it could reveal new insights into the behavior of nucleic acids in living beings. 7-Deaza-8-aza-adenine (4-aminopyrazolo-[3,4-d]pyrimidine, H4app) is a structural analogue of adenine (Hade) that has a fused pyrazole ring instead of an imidazole ring. Thus, it represents the translocation of the N7 and C8 atoms in Hade, according to purine conventional notation (see Scheme 1). This fact should perturb the proton tautomerism and the metal binding abilities of this former nucleobase. Indeed, the absence of the N7 residue in H4app, which is believed to be the most relevant metal binding site in natural purines (exposed at the major groove of DNA), has raised high and broad interest regarding its potential applications. In this context, several pharmacological properties have been already described for pyrazolo[3,4-d]pyrimidine ligands such as antibacterial and antifungal,[4] antiparasite,[5] or antiproliferative agents.[6] Likewise, they have been reported as adenosine

Received: October 2, 2012
Published: January 28, 2013

Scheme 1. (Top) Adenine and 4-Aminopyrazolo[3,4-d]pyrimidine with the Conventional Notation of Purines and (Bottom) Formulas of the Chelating Ligands Used in This Work: N-(p-Methylbenzyl)-iminodiacetate(2-) and N-(p-Fluorobenzyl)-iminodiacetate(2-) Anions (MEBIDA and FBIDA, Respectively)

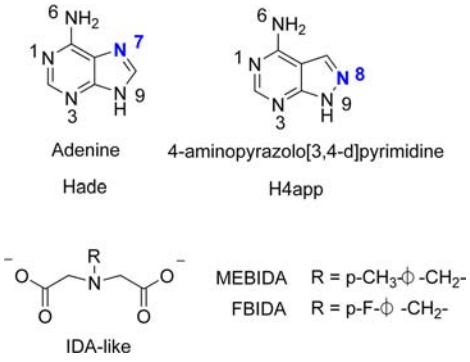

antagonists[7] and enzyme inhibitors.[8] However, further than these applications, the rationalization of the metal binding patterns in this kind of ligands is still necessary to better understand more complex processes concerning nucleic acids such as the role of metal ions in molecular crowding and their structural, functional, and stability consequences within biomolecules, for example concerning ribozymes.[9]

Under the structural point of view, the roles of H4app as ligand are rather unexplored. Some synthetic nucleosides derived from H4app have been isolated and characterized crystallographically.[10] Nevertheless, the existing data about H4app are mainly focused on three papers. Two independent solution studies[11,12] have provided two dissociation constants for 4-aminopyrazolo[3,4-d]pyrimidine ($pK_1 \sim 4.20$ and $pK_2 \sim 11$) attributable to the dissociations of protons placed on N1 and N9, respectively. Moreover, the study carried out by Dubois et al.[12] also provided energy calculations about the difference basicity of N9/N8. Therefore, the previous data suggest that the basicity order for the N-donors of H4app would be N9 ≥ N8 > N1 > N3 ≫ N6 (see Scheme 1). Alternatively, Sheldrick et al.[13] reported structural support about four metal binding patterns of H4app or its 4app and 4app-2H anionic forms, by increasing metalation with CH_3Hg-(I). Noticeably, the metal ion coordination observed therein is in good agreement with the N-basicity order proposed for this ligand. According to this panorama, in order to deepen our knowledge on the molecular recognition patterns of the nucleobase H4app, we have synthesized and characterized two novel mixed-ligand ternary copper(II) complexes with iminodiacetate-like chelators and H4app.

EXPERIMENTAL SECTION

Materials. Bluish $Cu_2CO_3(OH)_2$ was purchased from Probus. 4-Aminopyrazolo[3,4-d]pyrimidine (H4app) was purchased from Sigma-Aldrich. All the former reagents were used without further purification. N-(p-Methylbenzyl)- and N-(p-fluorobenzyl)-iminodiacetic acids (H_2MEBIDA and H_2FBIDA, respectively) were synthesized in their acid form as previously reported for N-benzyl-iminodiacetic acid[14] using 4-methyl-benzylamine (p-xylylamine) or 4-fluorobenzylamine instead of benzylamine, respectively.

Syntheses of the Complexes. *$[Cu_2(MEBIDA)_2(\mu_2\text{-}N1,N8\text{–}H4app)(H_2O)_2]\cdot 4H_2O$ (**1**).* $Cu_2CO_3(OH)_2$ (0.25 mmol, 0.055 g) was reacted in 50 mL of distilled water with H_2MEBIDA acid (0.5 mmol, 0.119 g) in a Kitasato flask, heating (50 °C) and stirring under moderate vacuum until a clear blue solution of the binary chelate was obtained. Alternatively, a suspension of H4app (0.5 mmol, 0.068 g) in 40 mL of isopropyl alcohol was prepared at r.t. Afterward, the suspension of H4app was added to the binary chelate solution, and the reacting mixture was stirred for 1 h until the reactants were completely dissolved. The resulting blue solution was filtered, without vacuum, on a crystallization device and allowed to stand at room temperature, covered with a plastic film to control the evaporation. After six weeks, needle-like crystals suitable for XRD purposes were collected. Yield is ca. 70–75%. Elemental analysis (%): Calc. for $C_{29}H_{43}Cu_2N_7O_{14}$: C 41.43, H 5.15, N 11.66; Found: C 41.83, H 5.24, N 11.77. FT-IR (KBr, cm-1) $\nu_{as}(H_2O)$ 3398, $\nu_{as}(NH_2)$ overshadowed, $\nu_s(NH_2)$ overlapped with $\nu_s(H_2O)$ 3247, ν(N–H) 3184, $\nu_{as}(CH_2)$ 2924, $\nu_s(CH_2)$ 2852, $\delta(H_2O)$ and $\delta(NH_2)$ overlapped with ν_{as}(COO) 1611, δ(N–H) 1517, ν_s(COO) 1384, $\pi(C\text{–}H)_{ar}$ 809 (MEBIDA), $\pi(C\text{–}H)_{ar}$ 788 (H4app). Under air-dry flow, the sample loses only 0.5 noncoordinated water molecule, thus the TG experiment starts with an average formula $[Cu_2(MEBIDA)_2(\mu_2\text{-}N1,N8\text{–}H4app)(H_2O)_2]\cdot 3.5H_2O$. The thermogravimetric curve shows five steps. The first step corresponds to the loss weight of the rest of water content (n = 5.5 H_2O; Calc. 12.03%; Found 12.07%). Indeed only H_2O and trace amounts of CO_2 are identified as evolved gases during this first step. The following pyrolitic steps yield a final residue of 2 CuO (470 °C, Calc. 19.31%; Found 20.77%). The evolved gases during the pyrolysis involve H_2O, CO_2, CO, and three N-oxide gases (N_2O, NO_2, and NO). See S-6 in the Supporting Information.

*$[Cu_4(FBIDA)_4(\mu_2\text{-}N8,N9\text{–}H4app)_2(H_2O)]\cdot 3.5H_2O$ (**2**).* A synthetic procedure similar to that of compound **1** was followed, using H_2FBIDA acid (0.5 mmol, 0.120 g) instead of H_2MEBIDA acid. The addition of isopropyl alcohol to the mother liquors is again needed to reach the complete solution of the ternary system. In two months, needle-like crystals were obtained. The reaction yielded 65%. Elemental analysis (%): Calc. for $C_{54}H_{59}Cu_4F_4N_{14}O_{20.5}$: C 41.51, H 3.81, N 12.55; Found: C 41.08, H 3.90, N 12.65. FT-IR (KBr, cm^{-1}) $\nu_{as}(H_2O)$ 3433, $\nu_{as}(NH_2)$ overshadowed, $\nu_s(NH_2)$ overlapped with $\nu_s(H_2O)$ 3232 ν(N–H) 3131 (sh), $\nu_{as}(CH_2)$ 2930, $\nu_s(CH_2)$ 2860, $\delta(H_2O)$ 1629, $\delta(NH_2)$ overlapped with ν_{as}(COO) 1606, δ(N–H) 1512, ν_s(COO) 1384, ν(C–F) 1005, $\pi(C\text{–}H)_{ar}$ 736 (FBIDA), $\pi(C\text{–}H)_{ar}$ 782 (H4app). The UV/vis spectrum shows an asymmetric d-d band with λ_{max} at 670 nm (ν_{max} 15000 cm^{-1}). Under air-dry flow, the sample loses part of the noncoordinated water molecule. Hence, the sample starts the TG experiment with formula $[Cu_4(FBIDA)_4(\mu_2\text{-}N8,N9\text{–}H4app)_2(H_2O)]\cdot 2.6H_2O$. The thermal behavior is divided in six steps. The sample loses all the water content during the first step (n = 3.60 H_2O; Calc. 4.21%; Found 4.20%), according to the evolved gases. Five additional pyrolitic steps produce H_2O, CO_2, CO, and N-oxide gases (N_2O, NO, NO_2) to finally reach an impure CuO residue (480 °C, Calc. 20.58%; Found 20.80%). See S-7 in the Supporting Information.

X-ray Structure Determinations. Measured crystals were prepared under inert conditions immersed in perfluoropolyether as protecting oil for manipulation. Suitable crystals were mounted on MiTeGen MicromountsTM, and these samples were used for data collection. Data were collected with Bruker X8 Proteum (compound **1**, 293 K) or Bruker SMART CCD 1000 (compound **2**, 110 K) diffractometers. The data were processed with SAINT[15] (**1**) or APEX2[16] (**2**) programs and corrected for absorption using SADABS.[17] The structures were solved by direct methods,[18] which revealed the position of all non-hydrogen atoms. These atoms were refined on F2 by a full-matrix least-squares procedure using anisotropic displacement parameters.[18] All hydrogen atoms were located in difference Fourier maps and included as fixed contributions riding on attached atoms with isotropic thermal displacement parameters 1.2 times those of the respective atom. Geometric calculations were carried out with PLATON,[19] and drawings were produced with PLATON[19] and MERCURY.[20] Additional crystal data and more information about the X-ray structural analyses are shown in Supporting Information S3 to S5. Crystallographic data for the structural analysis have been deposited with the Cambridge Crystallographic Data Centre, CCDC No. 881146 - 881147 for **1** and **2**, respectively. Copies of this

dx.doi.org/10.1021/ic302147u | Inorg. Chem. 2013, 52, 1916–1925

Table 1. DFT Gas Phase and Solvent (Water) Relative Gibbs Energies (ΔG_{rel}) for 4-Aminopyrazolo[3,4-d]pyrimidine, Calculated at the B3LYP/6-31+G**//B3LYP/6-31+G** and PCM-B3LYP/6-31+G**//PCM-B3LYP/6-31+G** Theoretical Levels, Respectively

compound	tautomer-H9 ΔG_{rel} (kcal/mol)	tautomer-H8 ΔG_{rel} (kcal/mol)	tautomer-H6 ΔG_{rel} (kcal/mol)	tautomer-H3 ΔG_{rel} (kcal/mol)	tautomer-H1 ΔG_{rel} (kcal/mol)
gas phase H4app	0.0	8.37	57.59	16.39	28.17
solvent(water) H4app	0.0	3.26	33.0	9.59	11.99

information may be obtained free of charge on application to CCDC, 12 Union Road, Cambridge CB2 1EZ, UK (fax: 44 1223 336 033; e-mail: deposit@ccdc.cam.ac.uk or http://www.ccdc.cam.ac.uk).

Computational Methods. DFT calculations, at the B3LYP[21] and unrestricted M06-L/6-31G* theoretical levels for the isolated H4app ligand and mononuclear copper complexes, respectively, have been performed with the Gaussian09 program,[22] using the 6-31+G** basis set, for the isolated ligands and the 6-31G* one for the copper complexes.[23] These methods have proven to be a reliable theoretical levels for the study of similar compounds.[24] All structures were fully optimized at the following theoretical levels: B3LYP/6-31+G**//B3LYP/6-31+G** for the isolated ligands and M06-L/6-31G*//M06-L/6-31G* for the copper(II) complexes. The most stable spin multiplicities for the mononuclear copper complexes studied were doublet. The local stability of all structures was checked through the eigenvalues of the matrix of second derivatives (Hessian); all energetic minima presented no imaginary frequencies. Solvent effect was taken into account by means of the self-consistent reaction field (SCRF) method, selecting PCM algorithm with water as solvent.[25] Additional information about DFT calculations is provided in Supporting Information S1 to S2.

Other Physical Methods. Analytical data were obtained in a Thermo-Scientific (Flash 2000) elemental microanalyzer. Infrared spectra were recorded by using KBr pellets on a Jasco FT-IR 6300 spectrometer. TG analyses were carried out in air-dry flow (100 mL/min) with a Shimadzu thermobalance TGA-DTG-50H instrument, coupled with a FT-IR Nicolet Magma 550 spectrometer. A series of FT-IR spectra (20−30 per sample) of the evolved gases were time-spaced recorded during the TG experiment. Diffuse reflectance (electronic) spectra were recorded in a Varian Cary-5E spectrophotometer. Variable temperature (2−300 K) magnetic susceptibility measurements on polycrystalline samples were carried out with a Quantum Design MPMS-7 SQUID magnetometer under a magnetic field of 0.1 T. The experimental susceptibilities were corrected for the diamagnetism of the constituent atoms by using Pascal's tables. X-band EPR measurements were carried out on a Bruker ELEXSYS 500 spectrometer with a maximum available microwave power of 200 mW and equipped with a superhigh-Q resonator ER-4123-SHQ. For Q-band studies, EPR spectra were recorded on a Bruker EMX system equipped with an ER-510-QT resonator and an ER-4112-HV liquid helium cryostat. The magnetic field was calibrated by a NMR probe, and the frequency inside the cavity was determined with a Hewlett-Packard 5352B microwave frequency counter. Computer simulation: WINEPR-Simfonia, version 1.5, Bruker Analytische Messtechnik GmbH).

RESULTS AND DISCUSSION

DFT Calculations. *Tautomers for 4-Aminopyrazolo[3,4-d]pyrimidine.* In order to explore the relative stability of the corresponding hydrogen tautomers of H4app, gas phase and solvent effect Gibbs energies have been calculated and summarized in Table 1. Since 4-aminopyrazolo[3,4-*d*]-pyrimidine is a bioisoster of adenine, it is expected that N9 remains as the most basic donor in the heterocycle, so that, in neutral form, we observe the H(N9)tautomer in gas phase and also when solvent effect is included. Indeed, the existence of the H(N9) tautomer as the most stable one is supported by solution data[11,12] and has also been described for other adenine derivatives such as azabenzimidazole ligands or deaza-adenine ligands.[24] Moreover, according to previous studies,[12] H(N8)-4app is the next stable tautomer, showing our calculations a small difference of 3.26 kcal·mol^{-1} in water compared to H(N9)4app. The H(N3)4app and H(N1)4app tautomers are higher in terms of ΔG_r (9.59 and 11.99 kcal·mol^{-1}, respectively), although they are rather close to each other. Moreover, it is noteworthy that, when solvent effect is taken into account in the calculations, all free Gibbs energy values are reduced significantly; i.e. the difference between the tautomer H(N1)4app in gas phase and H(N1)4app considering the solvent effect is 16.18 kcal·mol^{-1}.

Models for Mononuclear Copper(II) Complexes. With the aim of estimating the coordination abilities of H4app, DFT calculations have been carried out for ternary copper(II) model systems having the chelating ligand N-methyl-iminodiacetate(2-) anion (MIDA) and H4app. For all the calculations, a mer-NO_2 conformation was chosen for the iminodiacetate moiety and the binary chelate and the H4app ligand were induced to be coplanar, according to related structural results.[14,24] Moreover, the Cu(II)/MIDA chelate was tested for all the possible tautomers of H4app (see Tables S-1 and S-2 in the Supporting Information) since the presence of copper could alter the tautomeric preferences shown in Table 1 (vide supra). The most stable structure for the discrete system CuII/MIDA/H4app is the one having the most stable tautomer H(N9)4app. In this latter case, the Cu(II) atom is coordinated by N3(H4app) and assisted by an intramolecular H-bond N9−H···O(noncoord. carboxylate). Herein, the H4app and the MIDA chelating ligand remain coplanar, being the referred intramolecular interligand H-bond of maximum strength. However, for the same tautomer H(N9)4app and speaking in terms of solvent effect, two other possibilities, N1 or N8 coordination, are rather close in terms of free Gibbs energy to the aforementioned coordination via N3 (Figure 1). This fact points out the possibility of two additional molecular recognition patterns for H(N9)4app (ΔGr = 2.18 and 2.86 kcal·mol^{-1} for the N1 and N8 forms, respectively - see Table S-1 in the Supporting Information). Furthermore, the small difference between the two latter aforementioned patterns (0.68 kcal·mol^{-1}) suggests the possibility of the bidentate role μ_2-N1,N8 for H(N9)4app, as is indeed observed in compound **1** (see Results and Discussion).

If we extend the analysis of the Cu^{II}/MIDA/H4app model system to other H4app tautomers, different from H(N9)4app, then the lowest energetic value is 4 kcal·mol^{-1}. In particular, when we focus on the H(N1)4app tautomer, the three possible coordination modes are possible via N3, N8 or N9. Among them, only the N8 or N9 forms in H(N1)4app are likely to occur (see Table S-1 in the Supporting Information). Note that, although they show quite high ΔG_r values (11.28 and 10.08 kcal·mol^{-1}, respectively), the difference between these two values is rather small what could be indicative of a bidentate role for H(N1)4app tautomer, provided it is favored in more complex systems. In fact, the bidentate μ_2-N8,N9−

dx.doi.org/10.1021/ic302147u | Inorg. Chem. 2013, 52, 1916−1925

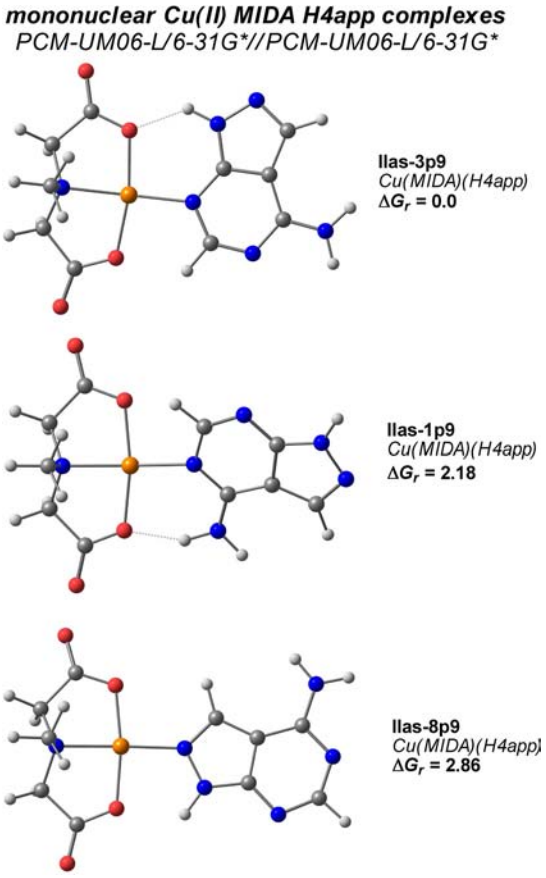

Figure 1. DFT (PCM-B3LYP/6-31G*//PCM-B3LYP/6-31G*) three most stable coordination modes for the mononuclear copper(II) complexes with the H(N9)4app tautomer and the chelating ligand MIDA. ΔG_r values in kcal·mol^{-1}.

H(N1)4app molecular recognition pattern has been proved by X-ray crystallography, not only in compound **2** but also in a pyrazolo[3,4-d]pyrimidin-4-one complex.[26]

The discrepancy between the DFT models and the experimental results may be related to the limitations of the mononuclear complexes. However, the above presented data enable the rationalization of the experimental results and highlight that both metal bindings are plausible in terms of energy.

Molecular and Crystal Structures. Compound **1**, with formula $[Cu_2(MEBIDA)_2(\mu_2\text{-N1,N8}-H4app)(H_2O)_2]\cdot 4H_2O$, consists of a centrosymmetric dinuclear complex molecule (Figure 2) and solvent water. In the complex, the copper(II) atoms exhibit a 4 + 1 coordination polyhedron where the four closest donor atoms correspond to the tridentate IDA-like chelating ligand MEBIDA (N10, O11, O21) and one N-donor (N1 or N8) from H4app (see Table S-3.2 in the Supporting Information). Thus, MEBIDA ligand adopts a mer-NO_2 conformation. The apical/distal coordination sites are occupied by aqua ligands which show rather short bond lengths [Cu1−O1 2.220(2) Å] in contrast to related apical distances which usually fall in the range of 2.3−2.6 Å. According to previous results, H4app shows its most stable tautomer H(N9)4app. Moreover, it acts as a bridging ligand displaying the unprecedented μ_2-N1,N8 mode. It is also remarkable that the coordination bond Cu−N1 is a bit longer than expected if we compare the present distance [Cu1−N1 2.109(2) Å] to those of Cu−N1(neutral purine) bonds available in the literature [i.e.,

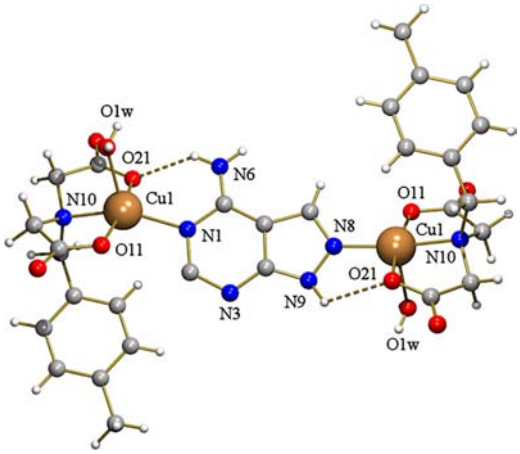

Figure 2. Complex molecule of $[Cu_2(MEBIDA)_2(\mu_2\text{-N1,N8}-H4app)(H_2O)_2]\cdot 4H_2O$ (**1**) with the numbering of the coordination environment. Only one of the two disordered positions is plotted for H4app. Solvent molecules omitted for clarity.

1.993(4) Å in μ_2-N1,N8−H7deaza-adenine in ref 24 or 2.020(2) Å in μ_2-N1,N9-Hade in ref 27].

Furthermore, both Cu−N1 and Cu−N8 bonds are assisted by the corresponding intramolecular interligand H-bonding interactions [N6−H6A···O21(carboxy coord., 3.091(7) Å, 136°) and N9−H···O21(carboxy coord., 2.975(3) Å, 119°)], respectively (see Figure 2). Note that the first interaction is a bit larger than usual (near to 3.1 Å), whereas the other has a rather low value angle (119°). The vagaries of these H-bonding interactions seem to be related to the implication of N6−H and N9−H groups in bifurcated intermolecular H-bonds. This fact may also contribute to the loss of planarity between the H4app ligand and the mean basal Cu^{II} coordination planes, displaying an open dihedral angle close to 40°. Furthermore, it should be noticed that, in the crystal, the ligand H4app is disordered over two positions, related to each other by an inversion center. This means that the H4app ligand is found in a special crystallographic position, and therefore each Cu^{II} center is 50% bonded to N1 or N8 (see Figure 3).

In the crystal of **1**, intermolecular pi,pi-stacking interactions between the aromatic ring of MEBIDA and the 5- and 6-

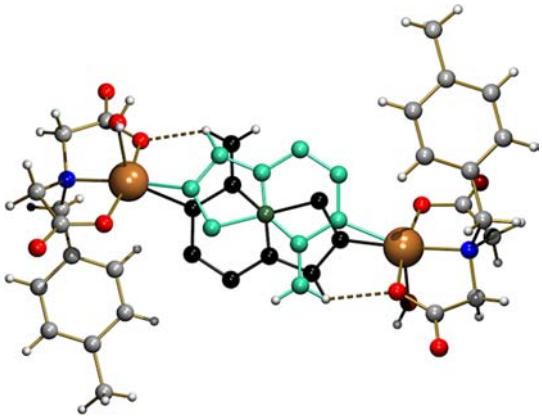

Figure 3. Complex molecule of $[Cu_2(MEBIDA)_2(\mu_2\text{-N1,N8}-H4app)(H_2O)_2]\cdot 4H_2O$ (**1**). The two disordered positions of H4app ligand are plotted in black and turquoise, respectively. The carbon atom shared by the two disordered position is depicted in dark green. Solvent molecules omitted for clarity.

dx.doi.org/10.1021/ic302147u | Inorg. Chem. 2013, 52, 1916−1925

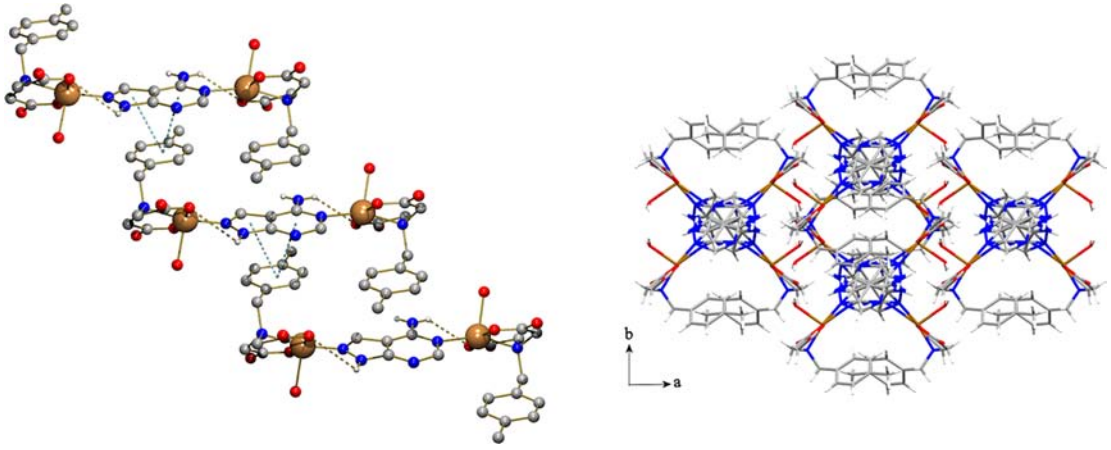

Figure 4. Left: detail of multistacked 1D chains in compound **1**. Only one of the two disordered positions for the H4app ligand is depicted for clarity. Right: View in the ba plane of the 3D honeycomb-like architecture in the crystal of **1**.

membered rings of H4app build multistacked chains that extend along the *b* axis (Figure 4, left) [geometrical stacking parameters: (i) Cg···Cg 3.628(3) Å, α = 3.2(3)°, β = 18.57°, γ = 21.38° and (ii) Cg···Cg 3.564(3) Å, α = 2.3(2)°, β = 13.11°, γ = 15.41°, respectively − see S-5.1 in the Supporting Information]. Adjacent chains connect to each other by intermolecular H-bonds that involve the apical aqua ligands and noncoordinated carboxylate O-atoms leading to a 3D honeycomb-like network (Figure 4, right - see also Table S-3.3 in the Supporting Information).

Compound **2** consists of an asymmetric tetranuclear complex molecule (Figure 5) and noncoordinated water molecules. The

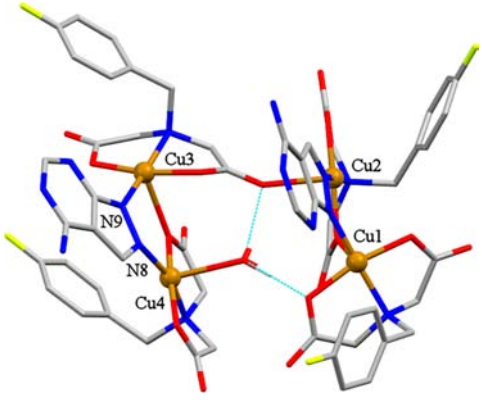

Figure 5. Complex molecule of $[Cu_4(FBIDA)_4(\mu_2\text{-N8,N9-H4app})_2(H_2O)]\cdot 3.5H_2O$ (**2**). Solvent molecules and H-atoms not involved in intramolecular H-bonding interactions are omitted for clarity.

four copper(II) centers show a square-based pyramidal coordination, type 4 + 1. Cu1 and Cu3 metal surroundings are of the same type. The donor atoms of the basal plane are supplied by a tridentate FBIDA chelator and the N9 atom of an H4app, whereas the apical sites are occupied by an O-monatomic μ_2-carboxylate atom. The Cu2 coordination is quite similar to those of Cu1 or Cu3, except for the apical O-atom that belongs to a syn,anti-μ_2-bridging carboxylate group. In contrast, the apical Cu4 site is remarkably occupied by one aqua ligand [Cu4−O(aqua) 2.463(3) Å]. Other selected bond lengths, interatomic distances, and angles are provided in Table S-4.2 in the Supporting Information. It should be noted that the FBIDA ligands play three different roles: (i) only as a tridentate chelator for Cu1; (ii) as tridentate chelator plus O-monatomic-μ_2-carboxylate ligand for Cu4; and (iii) as tridentate chelator and as a syn,anti-μ_2-O-O′-carboxylate ligand for Cu2 and Cu3. Herein, both H4app show a μ_2-N8,N9 bidentate role, using the H(N1)4app tautomer due to the transfer of the H(N9) atom to the N1 acceptor (the most basic N-donor atom available in the μ_2-N8,N9 coordination mode). Note that, in this conformation, the Cu−N(heterocyclic) bonds cannot cooperate with appropriate intramolecular interligand H-bonding interactions. This bridging μ_2-N8,N9 role was previously reported for methyl-Hg(I) derivatives of H4app, with formula $[(CH_3Hg)_2(\mu_2\text{-N8,N9−H(N1)4app})](NO_3)_2\cdot H_2O$.[13] Moreover, the H(N1) tautomer together with the μ_2-N8,N9 coordination role has been also described for one zinc(2+) complex of allopurinol (pyrazolo[3,4-d]pyrimidin-4-one).[26]

Interestingly, the complex molecule of **2** exhibits an unusual acyclic, nonlinear asymmetric topology, in which the apical aqua ligand of Cu4 plays two relevant roles. First, it restricts the nuclearity of the complex to four (instead of yielding, for example, a 1D polymer). Second, it determines the nonlinearity of the tetramer conformation by means of two intramolecular interligand H-bonds (Figure 5). In such interactions, the O(carboxylate) acceptors appertain to the FBIDA chelators of Cu1 [O4−H4A···O21(coord. carboxy), 2.905(4) Å, 140.5°] and Cu3 [O4−H4B···O16(non coord. carboxy), 2.757(4) Å, 165.1°]. This topology is in clear contrast to that of the cyclic-tetranuclear complex molecule found in $[Cu_4(pheida)_2(\mu_2\text{-O,O′-pheida})_2(\mu_2\text{-N3,N7−H(N9)ade})(H_2O)_2]\cdot 4H_2O$ (pheida = N-phenethyl-iminodiacetate(2-) ligand).[14] In this case, the cyclic topology is tied to the cooperation of the Cu−N3 and Cu−N7 bonds with appropriate intramolecular interligand N9−H···O(carboxy) and N6−H···O(carboxy) H-bonds and the μ_2-bridging role of two pheida ligands. Besides the above-mentioned H-bonds (vide supra), additional intermolecular H-bonds plus intra- and intermolecular pi,pi-stacking, ring-metal, X−H···ring, and X−Y···ring interactions are present in the crystal packing of compound **2**, contributing to the overall stabilization of the 3D network (Table 2 − see also Tables S-4.3 and S-5.2 in the Supporting Information). Among those interactions, the most significant ones are the following: (1) the pi,pi-stacking between the 6-membered rings of two H4app ligands (bridging Cu1 and Cu2) of adjacent tetrameric units (i = -x, 2-y, 1-z) and that involving the aromatic moieties from FBIDA chelators of Cu3 and Cu4 (ii = −1+x, y, z; iii =1+x, y, z)

dx.doi.org/10.1021/ic302147u | *Inorg. Chem.* 2013, 52, 1916−1925

Table 2. Relevant Distances (d) and Angles (α, β, γ) for the Different Intra- or Intermolecular Interactions Involving Aromatic Rings in the Crystal of Compound 2[f]

$\pi\cdots\pi$ interactions	centroid···centroid[a]	d[Cg(I)···Cg(J)] (Å)[b]	α (deg)[c]
	Cg(1)···Cg(1)^{i}	3.532	0.00
	Cg(2)···Cg(3)^{ii}	3.780	3.63
	Cg(3)···Cg(2)^{iii}	3.780	3.63
ring-metal interaction	centroid···metal	d[Cg(I)···Cu] (Å)	β (deg)[d]
	Cg(3)···Cu(4)	3.622	40.12
X–H···π interactions	X–H···centroid	d[H···Cg(I)] (Å)	γ (deg)[e]
	O(3)–H(3B)···Cg(4)^{iv}	2.83	21.95
	C(37)–H(37)···Cg(5)^{i}	2.83	7.65
X–Y···π interactions	X–Y···centroid	d[Y···Cg(I)] (Å)	γ (deg)
	C(45)–F(2)···Cg(6)^{v}	3.26	18.86
	C(22)–O(22)···Cg(7)	3.76	27.34
	C(26)–O(26)···Cg(2)	3.93	22.04

[a]Definition of centroids (Cg) corresponding to rings from 1 to 7: Cg(1) - (N51/C52/N53/C54/C55/C56); Cg(2) - (C62/C63/C64/C65/C66/C67); Cg(3) - (C72/C73/C74/C75/C76/C77); Cg(4) - (N58/N59/C54/C55/C57); Cg(5) - (N81/C82/N83/C84/C85/C86); Cg(6) - (C42/C43/C44/C45/C46/C47); Cg(7) - (C32/C33/C34/C35/C36/C37). The superscript lower case roman number within each interaction refers to the symmetry transformations: i = *-x, 2-y, 1-z*; ii = *−1+x, y, z*; iii = *1+x, y, z*; iv = *1+x, −1+y, z*; v = *−1-x, 2-y, -z*. [b]d[Cg(I)···Cg(J)]: distance between centroids of two different rings [i.e., (I), (J)]. [c]α: dihedral angle between the mean planes of rings (I) and (J). [d]β: angle between Cg(I)→Cu vector and normal to plane (I). [e]γ: angle between X–H vector and normal to plane (I). [f]For additional details see the appropriate Supporting Information (S5).

(Figure 6 - left). In the former interactions, the Cg···Cg distances are 3.53(1) and 3.78(1) Å, respectively, and the dihedral angles (α) are in the range of 0–4°, which are considered as rather intense pi,pi-stacking interactions (see S-5.2 in the Supporting Information).[28] (2) Likewise, it is remarkable the intramolecular ring-metal interaction observed between the aromatic moiety of the FBIDA(4) ligand and the related copper(II) center (Figure 6 - right), with a Cu4···Cg distance of 3.62(1) Å. Moreover, the distance metal-to-plane of 2.77(1) Å (from the normal to the mean plane of the ring, passing through the copper(II) atom) also reveals its significance. Such interaction is the only one present among the four possible alternatives within the tetranuclear unit, which underline the conformational versatility of the FBIDA ligands inside the tetramer.

Molecular Recognition Consequences. If we look over the broad structural information concerning adenine, in any of its forms, we will find that there are reported more than 50 structures in the Cambridge Structural Database that shows the M–N1 coordination bond. The vast majority of them comprise soft metal ions (such as Pt^{2+} or Ag^{+}) and N9-blocked adenine derivatives showing the bidentate μ_2-N1,N7 role, see for example ref 29. It is important to note that in 9-substituted purine ligands all the remaining N-donors are potential coordination sites since there are no tautomerism phenomena. However, if we focus on copper(II) ion, just five structures have been characterized displaying the Cu–N1 bond. Three of them correspond to one bridging μ_4-N1,N3,N7,N9-tetradentate adeninate(1-) anion[30] and two N9-blocked adenines with the aforementioned bridging μ_2-N1,N7 mode.[31] Interestingly, only two structures have neutral purine-like ligands: one is a mixed-ligand Cu-[μ_2-N1,N9–H(N7)ade] complex[27] and the other is a Cu-[μ_2-N1,N3–H(N9)7deaza-adenine] derivative recently characterized by our group.[24] Why the metal binding M–N1 is rarely described in solid state for neutral purine ligands still remains quite uncertain. Obviously the presence of the exocyclic amino group hinders the N1 atom, which is a poorer metal binding site in comparison to N7. However, equilibrium data published by Sigel et al.[32] concluded that purine residues may coordinate two metal ions simultaneously at N1 and N7 sites under physiological conditions. This fact is certainly of relevance and cannot be fully understood with the current knowledge. Thus, the relevance of **1** lies in the formation of the Cu–N1 bond, as a part of the μ_2-N1,N8 coordination mode displayed by H(N9)4app. Molecular recognition studies with purine analogues without the N7 atom, such as the previously referred H7deaza-adenine or H4app, point out the relevance of the N1/N7 dichotomy. In these latter ligands, the absence of the N7 donor seems to encourage the coordination abilities of the N-purine six-membered ring, and hence it turns N1 donor into a more attractive metal binding site. In compound **1** this is specially favored because (i) the metalation of N9 and N8

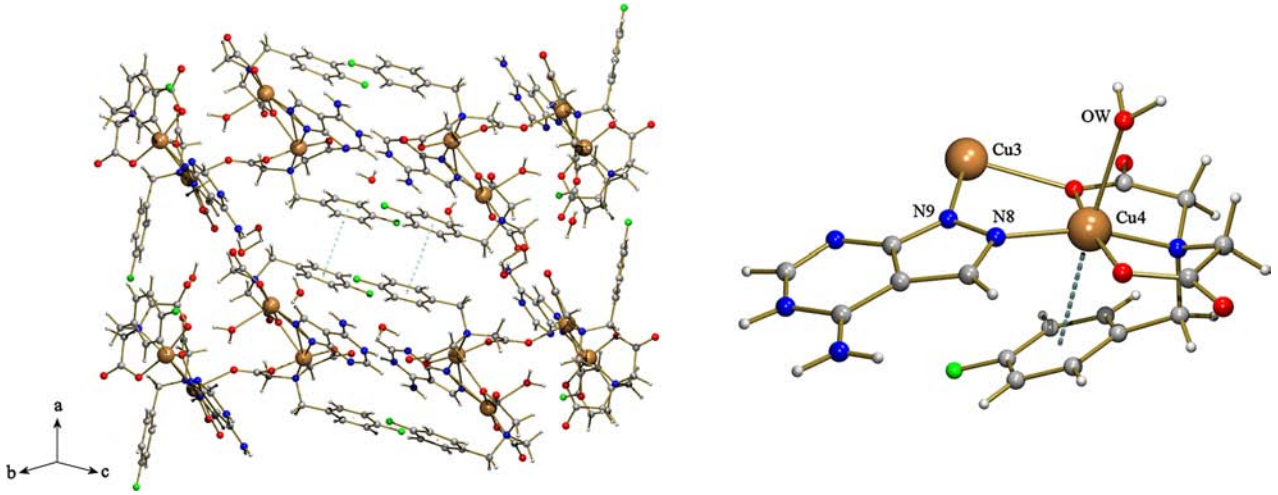

Figure 6. Left: view of unit cell of **2** showing pi,pi-stacking between phenyl groups of neighboring FBIDA ligands. Right: detail of metal-ring interaction within a fragment of the tetranuclear complex (**2**).

dx.doi.org/10.1021/ic302147u | *Inorg. Chem.* 2013, 52, 1916–1925

increases the acidity of N3 and (ii) in this mixed-ligand metal complex the N6−H bond can be involved in intramolecular interligand interaction that cooperates with the coordination bond. All this information may help us not only to better understand some processes in nature where purine ligands actively participate, especially larger oligonucleotides, but also to rationalize the molecular recognition processes in which this ligand, as part of new promising drugs, are involved.

Alternatively, another molecular recognition pattern has been described in compound **2** for the H4app ligand. Herein, the ligand uses the H(N1)4app tautomer and displays the μ_2-N8,N9 coordination mode. As we have commented previously, this role has been previously reported for H4app and its hydroxo-derivative allopurinol. It should be noted that, although the DFT calculations carried out in this study consider the use of the latter bridging mode, ΔG_r values were more favorable to the μ_2-N1,N8 bidentate role. This can be explained considering the difference in energy between the H(N9)4app and H(N1)4app tautomers, but also the vagaries of compound **2**, i.e. μ_2-N8,N9, cannot cooperate with intramolecular interligand H-bonding interactions. Anyhow, the molecular recognition patterns described for compounds **1** and **2** are in accordance with the assumed N-basicity order of H4app (N9 ≥ N8 > N1 > N3 ≫ N6), obtained from solution studies, and previous theoretical calculations (vide supra − see the DFT Calculations section). Going further on compound **2**, it is noteworthy how noncovalent interactions mainly drive the acyclic nonlinear topology of this tetranuclear complex molecule. In this compound, the unit corresponding to Cu4 plays an essential role controlling the nuclearity by means of intramolecular H-bonds that involve the apical aqua ligand. Besides this, it seems that the topology is further influenced by an unusual contribution of different intermolecular forces, from which it should be remarked the metal(Cu4)-ring interaction. This latter phenomenon is rather infrequent and of special relevance regarding the interaction of metal ions with biomolecules (i.e., blue copper proteins[33]).

EPR and Magnetic Properties. Since multinuclear compounds **1** and **2** have relevant stacking interactions within their molecular and crystal structures, X- and Q-band EPR measurements were carried out on powdered samples at several temperatures in the range 5−300 K. In all cases, the spin Hamiltonian parameters were estimated by comparison of the experimental spectra with those obtained by a computer simulation program working at the second order of the perturbation theory.

The X-band powder EPR spectrum of **1** has the characteristic shape of Cu(II) sites with rhombic symmetry (Figure 7). The main g-values are g_1 = 2.205, g_2 = 2.135, and g_3 = 2.048 (g_{iso} = 2.129), remaining practically unchanged from room temperature down to 5 K. The calculated G parameter[34] is 2.3, which indicates that the g values obtained from the experiment are not equal to the molecular ones. This fact implies the averaging by exchange coupling of the signal corresponding to magnetically nonequivalent copper sites, as Cu1 and Cu1e (1/2-x, −1/2+y, 1/2-z), connected via hydrogen bonding and separated by 7.8 Å (see Figure S-8.1 in the Supporting Information). The EPR line corresponds to a collective resonance when the exchange interaction (J) between copper ions in different lattice sites is larger than the difference between their Zeeman energies (0.3 cm^{-1} at X-band). However, on the Q-band EPR spectrum an additional rhombic signal is observed, with g'_1 = 2.269, g'_2 = 2.070, and g'_3 = 2.048 (g'_{iso} = 2.128). Considering that these g-values are molecular (G = 4.7), while the average parameter is practically the same in both signals, it can be concluded that the Q-band spectrum shows the simultaneous presence of collapsed and independent resonances for Cu1 and Cu1e sites. This is a rather uncommon behavior and implies that the condition $J_{Cu1-Cu1e} > |g_{Cu1}-g_{Cu1e}|\mu_B H$ does not hold for any orientation of the magnetic field operating at the Q-band.

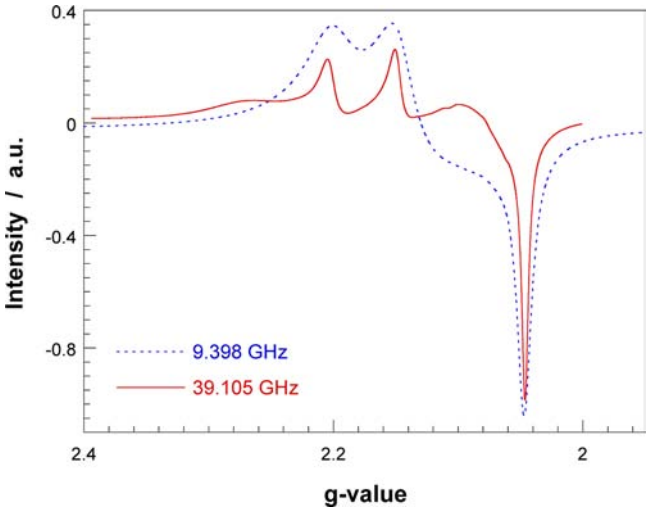

Figure 7. X- and Q-band powder EPR spectra of compound **1** registered at r.t.

Only one quasi-isotropic line, with g_{iso} = 2.13, is observed on the X- and Q-band powder EPR spectra of compound **2** registered at room temperature (see Figure S-8.2 in the Supporting Information). The intensity of this signal increases with decreasing temperature, reaching a maximum about 14 K after which it rapidly decreases. Below 20 K, two new satellite bands are observed at about 270 and 375 mT. At the same time, the classical "half-field signal" (ΔM_s = 2) is also detected. These results indicate that at room temperature EPR spectra are dominated by the characteristics of an S = 2 spin state, while a triplet state becomes more important below 20 K. Considering that the two satellite lines correspond to the perpendicular fine structure of the S = 1 state, the splitting between them yields the zero-field splitting parameter $|D|$ = 52 mT. The g value associated with this doublet is $g_\perp$ = 2.07. The zero-field interaction within the S = 2 state is small and hidden within the experimental line width. It is noteworthy that the observation of a fine structure at low temperatures indicates the absence of an appreciable magnetic exchange between tetrameric units.

The thermal variation of the inverse of the magnetic molar susceptibility (χ_m^{-1}) and the $\chi_m T$ product ($\mu_{eff}^2 = 8\chi_m T$) for compound **1** is shown in Figure 8. The effective magnetic moment exhibits a plateau from room temperature to 20 K having a value of 1.8 μ_B, decreasing to a value of 1.5 μ_B at 2 K. Above 10 K, the magnetic susceptibility follows a Curie−Weiss law with C_m = 0.86 cm^3 $Kmol^{-1}$ and θ = −0.7 K. Both, the negative temperature intercept and the decrease of the magnetic effective moment at low temperatures are in agreement with weak antiferromagnetic interactions in the compound. Taking into account the crystal structure the experimental data were fitted to the Bleaney−Bowers[35] expression [eq 1] for an isotropically coupled pair of S = 1/2 ions

dx.doi.org/10.1021/ic302147u | Inorg. Chem. 2013, 52, 1916−1925

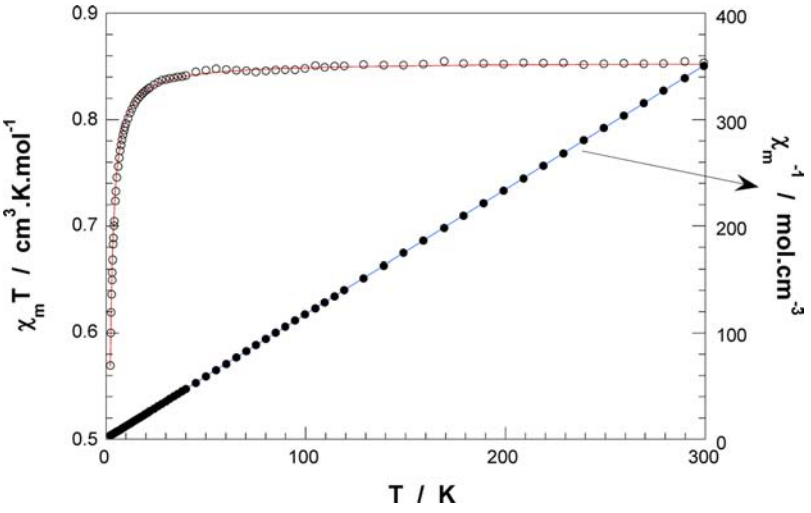

Figure 8. Thermal evolution of the reciprocal magnetic molar susceptibility χ_m^{-1} and the $\chi_m T$ product for compound **1**. The solid lines correspond to the best theoretical fits.

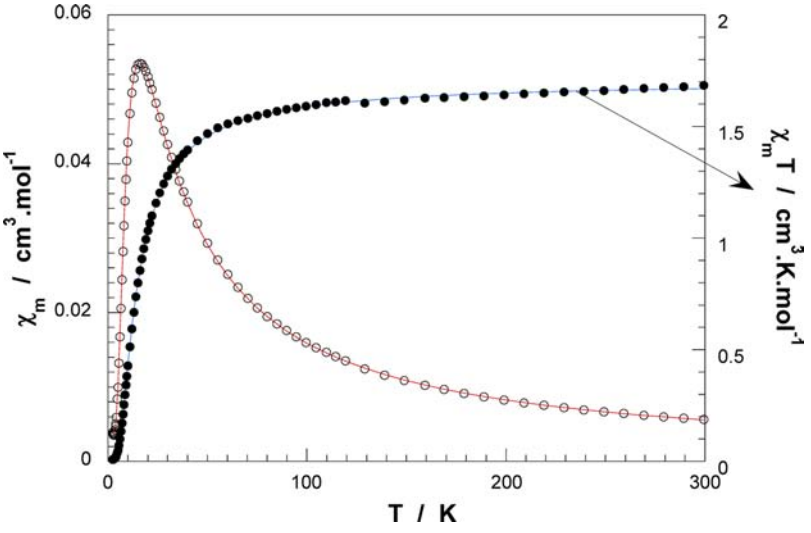

Figure 9. Plots of χ_m and $\chi_m T$ for compound **2**. The solid lines correspond to the best fit to eq 2.

$$\chi_m = \frac{Ng^2\beta^2}{kT(3 + 3\exp(-J/kT)} \quad (1)$$

where the singlet−triplet energy gap ($2J$) is defined by the Hamiltonian $H = -2J \cdot S_1 \cdot S_2$ ($S_1 = S_2 = 1/2$); g is the Lande's g factor; N, β, and k are Avogadro's number, the Bohr magneton, and Boltzmann's constant, respectively. The best-fit parameters obtained by minimizing the reliability factor $R = \Sigma[(\chi_m T)_{exp} - (\chi_m T)_{cal}]^2/\Sigma[(\chi_m T)_{exp}]^2$ are $g = 2.13$, $J = -0.8$ cm^{-1}, and $R = 6.1 \times 10^{-5}$. As shown in Figure 8, calculated curves reproduce satisfactorily the experimental data in the whole investigated temperature range. The low value of the calculated coupling parameter is in good agreement with the long exchange pathway via the H4app ligand.

The thermal evolutions of both the magnetic molar susceptibility and $\chi_m T$ values for compound **2** are shown in Figure 9. At room temperature, $\chi_m T$ is equal to 1.68 cm^3 mol^{-1}K, a value that is only slightly lower than that expected for a set of four magnetically noninteracting copper(II) ions (ca. 1.70 cm^3 mol^{-1} K using the $<g>$ = 2.13 value obtained from the EPR data). Upon cooling, $\chi_m T$ continuously decreases, and it practically vanishes at very low temperatures. As the temperature is lowered the susceptibility increases until a maximum of 0.0535 cm^3 mol^{-1}, which is reached at about 16 K, and then rapidly decreases (0.0035 cm^3 mol^{-1} at 3 K). The susceptibility increases below 3 K, probably due to the presence of a small paramagnetic impurity. At high temperature, $T \geq 100$ K, the thermal evolution of χ_m follows the classical Curie−Weiss law, with Weiss temperature $\theta = -8.5$ K and Curie constant $C_m = 1.72$ cm^3 mol^{-1} K. These results confirm the prevalence of antiferromagnetic interactions in this compound.

To interpret quantitatively the magnetic data we had analyzed them in terms of the "dipolar coupling" approach for a Cu(II) tetrameric compound. With the numbering scheme used in Figure 2, the Heisenberg spin Hamiltonian appropriate for the exchange interaction in this system can be written as

$$H = -2J_1(S_1 \cdot S_2 + S_3 \cdot S_4) - 2J_2(S_2 \cdot S_3)$$

where J_1 describes the nearest neighbor interaction between the outer pairs of copper and J_2 the central exchange constant. Interactions between non-nearest neighbors or via hydrogen bonds have been neglected to avoid an excessive number of adjustable parameters. The eigenvalues derived from this

dx.doi.org/10.1021/ic302147u | Inorg. Chem. 2013, 52, 1916−1925

Hamiltonian[36] were introduced in the van Vleck equation[37] to obtain an analytical expression for the magnetic susceptibility. An additional term (ρ) which accounts for uncoupled Cu(II) ions following a simple Curie law and having the same g factor has been also included [eq 2]:

$$\chi_m = (1-\rho)\frac{Ng^2\beta^2}{3kT}\frac{\sum_i S_i(S_i+1)(2S_i+1)\exp\left(-\frac{E_i}{kT}\right)}{\sum_i (2S_i+1)\exp\left(-\frac{E_i}{kT}\right)} + 4\rho\frac{Ng^2\beta^2}{4kT} \quad (2)$$

The best fit to the data were obtained with $J_1 = -8.9$ cm^{-1}, $J_2 = -0.8$ cm^{-1}, $g = 2.14$, and $\rho = 0.007$ ($R = 2.5 \times 10^{-5}$). The calculated J values imply that the ground state of this cluster is $S = 0$, but two $S = 1$ triplet states are only a few Kelvin over the singlet, in good agreement with the spin triplet signals observed in the EPR spectra at low temperatures.

CONCLUDING REMARKS

The crystallographic and DFT theoretical results presented herein are in good agreement and indicate that the N7/C8 translocation still allows a high versatility in the coordination abilities of H4app compared to adenine. In particular, H4app enables two bridging coordination modes, namely μ_2-N1,N8 and μ_2-N8,N9 for H(N9)4app and H(N1)4app, respectively. In contrast to the metal binding behavior of adenine, our findings suggest that the metal binding to the N1 donor in H4app is favored. In addition, the coordination ability of N8 in H4app should be also remarked. In conclusion, the study of the molecular recognition patterns of this kind of ligands can provide new insights into the metal binding behavior of purines within biological systems (via nature or any anthropogenic way, i.e. drugs). These results not only might be of interest concerning "metal crowding" in larger oligonucleotides but also can help to rationalize the design of new promising drugs derived from pyrazolo[3,4-d]pyrimidines.

ASSOCIATED CONTENT

Supporting Information

Calculated Gibbs free energies of all the analyzed compounds as well as extra DFT information are detailed in S-1 and S-2. Additional structural information is provided in S-3 to S-5 (CCDC 881146 - 881147). Relevant spectral properties and thermal stability information as well as magnetic properties can be found in S-6, S-7, and S-8, respectively. This material is available free of charge via the Internet at http://pubs.acs.org.

AUTHOR INFORMATION

Corresponding Author

*Phone: +34 958 24 38 53. Fax: +34 958 24 62 19. E-mail: adominguez@ugr.es.

Notes

The authors declare no competing financial interest.

ACKNOWLEDGMENTS

Financial support from Research Groups FQM-283 and FQM-174 (Junta de Andalucía) and MICINN-Spain (Project MAT2010-15594) is acknowledged. The project 'Factoría de Cristalización, CONSOLIDER INGENIO-2010' provided X-ray structural facilities for this work. We thank the "Centro de Servicios de Informática y Redes de Comunicaciones" (CSIRC), Universidad de Granada, for providing computing time. Financial support from ERDF Funds and Junta de Andalucía to acquire the FT-IR spectrophotometer Jasco 6300 is acknowledged. A.D.M. gratefully acknowledges ME-Spain for a FPU Ph.D contract.

REFERENCES

(1) (a) Sigel, H. *Pure Appl. Chem.* **2004**, *76*, 1869−1886. (b) Terrón, A.; Fiol, J. J.; García-Raso, A.; Barcelo-Oliver, M.; Moreno, V. *Coord. Chem. Rev.* **2007**, *251*, 1973. (c) Choquesillo-Lazarte, D.; Brandi-Blanco, M. P.; García-Santos, I.; González-Pérez, J. M.; Castiñeiras, A.; Niclós-Gutiérrez, J. *Coord. Chem. Rev.* **2008**, *252*, 1241. (d) Lippert, B. *Nucleic Acid - Metal Ion Interactions*; Hud, N. V., Ed.; RSC Publishing: London, 2009; Chapter 2.

(2) Patel, D. K.; Domínguez-Martín, A.; Brandi-Blanco, M. P.; Choquesillo-Lazarte, D.; Nurchi, V. M.; Niclós-Gutiérrez, J. *Coord. Chem. Rev.* **2012**, *256*, 193.

(3) (a) Choquesillo-Lazarte, D.; Domínguez-Martín, A.; Matilla-Hernández, A.; Sánchez de Medina Revilla, C.; González-Pérez, J. M.; Castiñeiras, A.; Niclós-Gutiérrez, J. *Polyhedron* **2010**, *29*, 170. (b) Patel, D. K.; Choquesillo-Lazarte, D.; Domínguez-Martín, A.; Brandi-Blanco, M. P.; González-Pérez, J. M.; Castiñeiras, A.; Niclós-Gutiérrez, J. *Inorg. Chem.* **2011**, *50*, 10549. (c) Domínguez-Martín, A.; Cho-quesillo-Lazarte, D.; González-Pérez, J. M.; Castiñeiras, A.; Niclós-Gutiérrez, J. *J. Inorg. Biochem.* **2011**, *105*, 1073.

(4) Holla, B. S.; Mahalinga, M.; Karthikeyan, M. S.; Akberali, P. M.; Shetty, N. S. *Bioorg. Med. Chem.* **2006**, *14*, 2040.

(5) Hasan, A.; Satyanarayana, M.; Mishra, A.; Bhakuni, D. S.; Pratap, R.; Dube, A.; Guru, P. Y. *Nucleosides, Nucleotides Nucleic Acids* **2006**, *25*, 55.

(6) (a) Carraro, F.; Naldini, A.; Pucci, A.; Locatelli, G. A.; Maga, G.; Schenone, S.; Bruno, O.; Ranise, A.; Bondavalli, F.; Brullo, C.; Fossa, P.; Menozzi, G.; Mosti, L.; Modugno, M.; Tintori, C.; Manetti, F.; Botta, M. *J. Med. Chem.* **2006**, *49*, 1549−1561. (b) Franco, L.; Davide, D. F.; Stevens, M. R. PCT Int. Appl. WO2011014239 (A1) 2011. (c) Indovina, P.; Giorgi, F.; Rizzo, V.; Khadang, B.; Schenone, S.; Di Marzo, D.; Forte, I. M.; Tomei, V.; Mattioli, E.; D'Urso, V.; Grilli, B.; Botta, M.; Giordano, A.; Pentimalli, F. *Oncogene* **2012**, *31*, 929.

(7) Davies, L. P.; Brown, D. J.; Chow, S. C.; Johnston, G. A. R. *Neurosci. Lett.* **1983**, *41*, 189.

(8) (a) Da Settimo, F.; Primofiore, G.; La Motta, C.; Taliani, S.; Simorini, F.; Marini, A. M.; Mugnaini, L.; Lavecchia, A.; Novellino, E.; Tuscano, D.; Martini, C. *J. Med. Chem.* **2005**, *48*, 5162−5174. (b) Hsieh, J.-F.; Wu, S.-H.; Yang, Y.-L.; Choong, K.-F.; Chen, S.-T. *Bioorg. Med. Chem.* **2007**, *15*, 3450−3456.

(9) Nakano, S.; Karimata, H. T.; Kitagawa, Y.; Sugimoto, N. *J. Am. Chem. Soc.* **2009**, *131*, 16881.

(10) (a) Sprang, S.; Scheller, R.; Rohrer, D.; Sundaralingam, M. *J. Am. Chem. Soc.* **1978**, *100*, 2867. (b) Seela, F.; Zulauf, M.; Reuter, H.; Kastner, G. *Acta Crystallogr., Sect. C: Cryst. Struct. Commun.* **1999**, *C55*, 1947. (c) Zhang, X.; Budow, S.; Leonard, P.; Eickmeier, H.; Seela, F. *Acta Crystallogr., Sect. C: Cryst. Struct. Commun.* **2006**, *C62*, o79. (d) Pasternak, A.; Kierzek, R.; Gdaniec, Z.; Gdaniec, M. *Acta Crystallogr., Sect. C: Cryst. Struct. Commun.* **2008**, *C64*, o467.

(11) Casper, A.; Fazakerley, V. *J. Chem. Soc., Dalton Trans.* **1975**, 1977−1980.

(12) Dodin, G.; Dreyfus, M.; Bensaude, O.; Dubois, J.-E. *J. Am. Chem. Soc.* **1977**, *99*, 7257.

(13) Sheldrick, W. S.; Bell, P.; Hausler, H.-J. *Inorg. Chim. Acta* **1989**, *163*, 181−192.

(14) Bugella-Altamirano, E.; Choquesillo-Lazarte, D.; González-Pérez, J. M.; Sánchez-Moreno, M. J.; Marín-Sánchez, R.; Martín-Ramos, J. D.; Covelo, B.; Carballo, R.; Castiñeiras, A.; Niclós-Gutiérrez, J. *Inorg. Chim. Acta* **2002**, *339*, 160.

(15) BRUKER, *SMART and SAINT. Area Detector control and Integration Software*; Bruker Analytical X-ray Instruments Inc.: Madison, WI, USA, 1997.

(16) BRUKER, *APEX2 Software, V.2010.11*; Bruker AXS Inc.: Madison, WI, USA.
(17) Sheldrick, G. M. *SADABS, Program for Empirical Absorption Correction of Area Detector Data*; University of Göttingen: Germany, 2009.
(18) Sheldrick, G. M. *Acta Crystallogr., Sect. A: Found. Crystallogr.* **2008**, *A64*, 112.
(19) Spek, A. L. *PLATON. A Multipurpose Crystallographic Tool*; Utrecht University: Utrecht, The Netherlands, 2010.
(20) Macrae, C. F.; Bruno, I. J.; Chisholm, J. A.; Edgington, P. R.; McCabe, P.; Pidcock, E.; Rodriguez-Monge, L.; Taylor, R.; van de Streek, J.; Wood, P. A. *J. Appl. Crystallogr.* **2008**, *41*, 466.
(21) Becke, A. D. *J. Chem. Phys.* **1993**, *98*, 5648.
(22) Frisch, M. J.; Trucks, G. W.; Schlegel, H. B.; Scuseria, G. E.; Robb, M. A.; Cheeseman, J. R.; Scalmani, G.; Barone, V.; Mennucci, B.; Petersson, G. A.; Nakatsuji, H.; Caricato, M.; Li, X.; Hratchian, H. P.; Izmaylov, A. F.; Bloino, J.; Zheng, G.; Sonnenberg, J. L.; Hada, M.; Ehara, M.; Toyota, K.; Fukuda, R.; Hasegawa, J.; Ishida, M.; Nakajima, T.; Honda, Y.; Kitao, O.; Nakai, H.; Vreven, T.; Montgomery, J. A., Jr.; Peralta, J. E.; Ogliaro, F.; Bearpark, M.; Heyd, J. J.; Brothers, E.; Kudin, K. N.; Staroverov, V. N.; Keith, T.; Kobayashi, R.; Normand, J.; Raghavachari, K.; Rendell, A.; Burant, J. C.; Iyengar, S. S.; Tomasi, J.; Cossi, M.; Rega, N.; Millam, J. M.; Klene, M.; Knox, J. E.; Cross, J. B.; Bakken, V.; Adamo, C.; Jaramillo, J.; Gomperts, R.; Stratmann, R. E.; Yazyev, O.; Austin, A. J.; Cammi, R.; Pomelli, C.; Ochterski, J. W.; Martin, R. L.; Morokuma, K.; Zakrzewski, V. G.; Voth, G. A.; Salvador, P.; Dannenberg, J. J.; Dapprich, S.; Daniels, A. D.; Farkas, O.; Foresman, J. B.; Ortiz, J. V.; Cioslowski, J.; Fox, D. J. *Gaussian 09, Revision B.01*;Gaussian, Inc.: Wallingford, CT, 2010.
(23) Hehre, W. J.; Ditchfield, R.; Pople, J. A. *J. Chem. Phys.* **1972**, *56*, 2257.
(24) Domínguez-Martín, A.; Choquesillo-Lazarte, D.; Dobado, J. A.; Vidal, I.; González-Pérez, J. M.; Castiñeiras, A.; Niclós-Gutiérrez, J. *Dalton Trans.* **2012**, DOI: 10.1039/c2dt32191b.
(25) Miertuš, S.; Scrocco, E.; Tomasi, J. *Chem. Phys.* **1981**, *55*, 117.
(26) Hänggi, G.; Schmalle, H.; Dubler, E. *J. Chem. Soc., Dalton Trans.* **1993**, 941.
(27) Das, S.; Madhavaiah, C.; Verma, S.; Bharadwaj, P. K. *Inorg. Chim. Acta* **2005**, *358*, 3236.
(28) Janiak, C. *J. Chem. Soc., Dalton Trans.* **2000**, 3885.
(29) (a) Roitzsch, M.; Lippert, B. *Chem. Commun.* **2005**, 5991. (b) Roitzsch, M.; Lippert, B. *Inorg. Chem.* **2004**, *43*, 5483. (c) Purohit, C. S.; Verma, S. *J. Am. Chem. Soc.* **2007**, *129*, 3488.
(30) Yang, E.-C.; Zhao, H.-K.; Feng, Y.; Zhao, X.-J. *Inorg.Chem.* **2009**, *48*, 3511.
(31) (a) Srivatsan, S. G.; Parvez, M.; Verma, S. *Chem.—Eur. J.* **2002**, *8*, 5184. (b) Prajapati, R. K.; Verma, S. *Inorg. Chem.* **2011**, *50*, 3180.
(32) Knobloch, B.; Sigel, R. K. O.; Lippert, B.; Sigel, H. *Angew. Chem., Int. Ed.* **2004**, *43*, 3793.
(33) Abdelhamid, R. F.; Obara, Y.; Uchida, Y.; Kohzuma, T.; Dooley, D. M.; Brown, D. E.; Hori, H. *J. Biol. Inorg. Chem.* **2007**, *12*, 165.
(34) Hathaway, B. J.; Billing, D. *Coord. Chem. Rev.* **1970**, *5*, 143.
(35) Bleaney, B.; Bowers, K. D. *Proc. R. Soc. London, Ser. A* **1952**, *214*, 451.
(36) Papadopoulos, A. N.; Tangoulis, V.; Raptopoulou, C. P.; Terzis, A.; Kessissoglou, D. P. *Inorg. Chem.* **1996**, *35*, 559.
(37) Van Vleck, J. H. *Theory of Electric and Magnetic Susceptibilities*; Oxford University Press: 1932.